RSC Advances

PAPER

View Article Online
View Journal | View Issue

Cite this: *RSC Adv.*, 2019, **9**, 30503

One-step formation of infrared reflection microsheets *via* local photo-induced *in situ* polymerization

Jingxing Zhang,†[ab] Zekun Guo,†[ab] Yancong Feng,[ab] Yao Wang,[ab] Hao Li*[ab] and Guofu Zhou[ab]

Received 13th June 2019
Accepted 9th September 2019

DOI: 10.1039/c9ra04453a

rsc.li/rsc-advances

Liquid crystal (LC) smart windows with adjustable reflectivity have been gradually applied in green and intelligent building materials for energy saving needs, but their applications are limited by their fundamental defects. In this study, we developed local photo-induced *in situ* polymerization to rapidly fabricate the infrared reflection microsheets of a cholesteric LC polymer as functional units. With the exception of the LC formula, the photo mask, liquid crystal cell, polymerization inhibitor, and the preparation conditions were specifically managed to control the extent of *in situ* polymerization, namely the microsheet morphology. The circular, triangular and oval-shaped microsheets were precisely obtained and were slightly bigger than the light hole. This easy, controllable, continuous and recyclable technology is expected to promote the industrialization of a high quality LC smart window with an adjustable reflection band and state.

Introduction

As a new generation of green building materials, smart windows have gradually developed from a simple light modulator to a comprehensive conditioner of indoor environments.[1,2] They can absorb or reflect solar radiation with specific wavelengths to adjust the indoor lighting or temperature for energy-saving needs.[3] The two common categories of smart windows are the non-adjustable smart windows (*e.g.*, low-emittance coatings[4,5] and dielectric/metal/dielectric (D/M/D) films[6,7]) and the adjustable ones (*e.g.*, electrochromic,[8–11] gasochromic,[12] photochromic and thermo-chromic[13] smart windows).

In particular, adjustable particle-suspended[14] and liquid crystal (LC) glazing smart windows[15] have started to come into daily applications. The former is performed by overturning or shifting the suspended particles in the applied physical field. Their high efficiencies are mainly determined by the particle size, shape and formula.[16,17] However, they commonly possess reflectivity in the full light band, unlike the LC ones with a reflection band that can be regulated.[18,19] For the latter one, either a reliable polymer-stabilized LC (PSLC) or a sensitive polymer-dispersed LC (PDLC) smart window is generally dependent on the LC phase transition under the stimulus of applied physical signals to change the overall optical properties.[20–23] Their fundamental defect is that their transmittances are strictly limited by the circular polarization and viewing angle. More specifically, PSLC is greatly affected by the inner cross-linked network in the response rate, and PDLC is only used for converting visible transparency.[24–27]

In the present study, we developed a rapid, controllable, continuous and recyclable preparation method for the one-step formation of cholesteric liquid crystal polymer (CLCP) microsheets for smart windows. Here, a local photo-induced *in situ* polymerization (LPISP) combined with a specific hole-array photomask was applied to control the microsheet morphology. This approach can integrate a few advantages of various smart windows into a single device. Alternatively, it makes those generated LC microsheets featuring an adjustable reflection band and a stable cross-linked structure such as PSLC, and is also available to a particle-suspended smart window with a higher response rate. Specifically, it is expected to provide a novel feasibility to the industrial production of adjustable LC smart windows.

Experimental

Materials

D-Glucitol,1,4:3,6-dianhydro-2,5-bis[4-[[4-[[[4-[(1-oxo-2-propen-1-yl)oxy]butoxy]carbonyl]oxy]benzoyl]oxy]benzoate] (98%, cross-linker), 2-methyl-1,4-phenylene bis(4-(3-(acryloyloxy)propoxy) benzoate) (98%, monomer A), 4-(6-acryloyloxy-hexyloxy)-benzoic acid 4-cyano-phenyl ester (98%, monomer B), and 4-(6-acryloyloxy-hexyloxy)-benzoic acid 4-methoxy-phenyl ester

[a]*Guangdong Provincial Key Laboratory of Optical Information Materials and Technology, Institute of Electronic Paper Displays, South China Academy of Advanced Optoelectronics, South China Normal University, Guangzhou 510006, China*
[b]*National Center for International Research on Green Optoelectronics, South China Normal University, Guangzhou 510006, China*
† These authors contributed equally to this work.

(98%, chiral dopant) were purchased from Jiangsu China Hecheng Display Technology Co., Ltd. (Nanjing, P. R. China). Phenylbis(2,4,6-trimethylbenzoyl)phosphine oxide (99%, photoinitiator 819) was purchased from Heowns Biochem Technologies Ltd. (Tianjin, P. R. China). Polyvinyl alcohol (PVA; 78% hydrolyzed, 6000 g mol^{-1}), hydroquinone (99%, inhibitor). The gap control spacer (SP-215, 15 μm) was purchased from SEKISUI Chemical Co., Ltd. (Osaka, Japan). All other reagents and organic solvents were of analytic reagent (AR) grade without any further treatment prior to use.

In addition, ultra-clear (transmittance 550 nm: ~94%) and ITO glass plates (area resistance: <10 Ω sq^{-1}; transmittance 550 nm: ~77%) with the same thickness of 1.1 mm were obtained from Luoyang Guluoglass Co., Ltd. (Luoyang, P. R. China). The pattern photomasks (size: 50 mm × 50 mm × 1.1 mm) with different hole arrays, including the circle hole (size: 15, 30, and 60 μm; pitch: 250, 300, and 350 μm), regular triangle hole (side length: 81 μm), oval hole (long axis: 85 μm; short axis: 42 μm) and circle-inscribed pentagon hole (diameter: 102 μm) with an equal area to that of the 60 μm-wide circle, were purchased from Kelead Photoelectric Materials Co., Ltd. (Shenzhen, P. R. China). Two round hole sieves (stainless steel 304; diameter: 10 cm) with 110 (hole size: 150 μm) and 1000 (hole size: 15 μm) meshes, respectively, were purchased from Taizhou Yueyang Trading Co., Ltd. (Taizhou, P. R. China).

Preparation of CLCP microsheets

The CLCP microsheets with different reflection bands were prepared *via* LPISP (see Fig. 1). Typically, a liquid crystal cell was first constructed by two parallel ultraclear glass plates (3.0 cm × 3.0 cm) with a fixed spacing distance (15 μm, determined by a gap control spacer). Here, the vertically aligned layer was coated on the glass substrate by spin coating a PVA aqueous solution (5 wt%), using a spin coater (KW-4A, Institute of Microelectronics of the Chinese Academy of Sciences, Beijing, P. R. China) with a fixed rotating speed of 2000 rpm for 30 seconds. Subsequently, the PVA layer was heated to 60 °C for 1 hour *via* a heating stage (JF-956A, Dongguan Changan Jinfeng Electronic Tools Factory, Dongguan, P. R. China), and then rubbed unidirectionally by a polyester fabric for alignment. The raw materials of CLCP with the previously reported formula[28–31] (see Fig. 2) were preheated up to 80 °C in the isotropic state. Once filled into the liquid crystal cell and cooled to about 50 °C, the mixture was cured locally under the cover of the pattern photomask by ultraviolet-visible (UV-Vis) light (wavelength range: 320–500 nm) with a fixed intensity of 0.1 W cm^{-2} (OmniCure S1500A, Lumen Dynamics Group Inc., Mississauga, Canada) for 30 seconds. Here, the photomask was pressed close to the cover glass plate to reduce diffraction and refraction effects. Finally, the resulting microsheets were collected in a dichloromethane (CH_2Cl_2) dispersion by filtering twice using the round hole sieves with 110 and 1000 meshes, respectively. After the removal of CH_2Cl_2, the residual unpolymerized LC mixture can be recycled in the next production process.

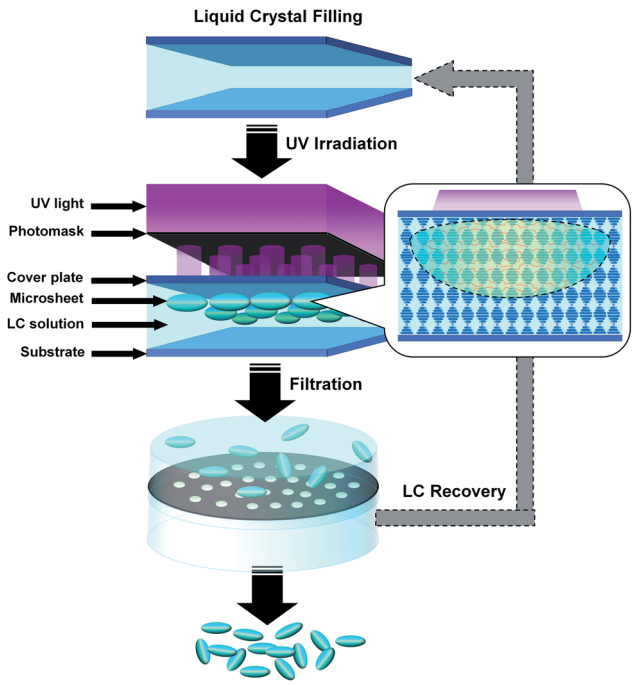

Fig. 1 Schematic on the production process of the CLCP microsheets *via* LPISP.

Characterizations

The ultraviolet-visible-near infrared (UV-Vis-NIR) reflectivity was tested using a fiber optic spectrometer (FOIS-1, Ocean Optics (Shanghai) Co., Ltd., Shanghai, P. R. China). Optical images were photographed using a polarizing optical microscope (POM; Leica DM2700P, Leica Microsystems Inc., Wetzlar, Germany) at room temperature. Surface topography was recorded using a 3D profiler (Leica DCM8, Leica Microsystems Inc., Wetzlar, Germany).

Results and discussion

CLCP formula

It is well-known that the cholesteric liquid crystal (CLC) behaving like regular chiral helixes possesses unique optical features. Typically, its reflection role is derived from the Bragger reflection under the Fergason reflection model as defined by the following equation:[32,33]

$$\lambda = \bar{n}p \quad (1)$$

where λ is the reflection wavelength, n is the mean refractive index of CLC, and p is the pitch of the CLC helix. Clearly, λ is proportional to p. Alternatively, the variation in p will greatly affect the reflection band of CLC. Therefore, we adjusted the component proportion to change the p value for the determined reflection band on the basis of the original CLC formula[28–31] (see Fig. 2).

In Fig. 3, the two fully cured CLCP films displayed an obvious reflectivity to the incident light with the visible (Vis) and near-infrared (NIR) light ranges. The reflectivity maximum of the Vis CLCP formula was below 10% in the NIR range from 750 nm

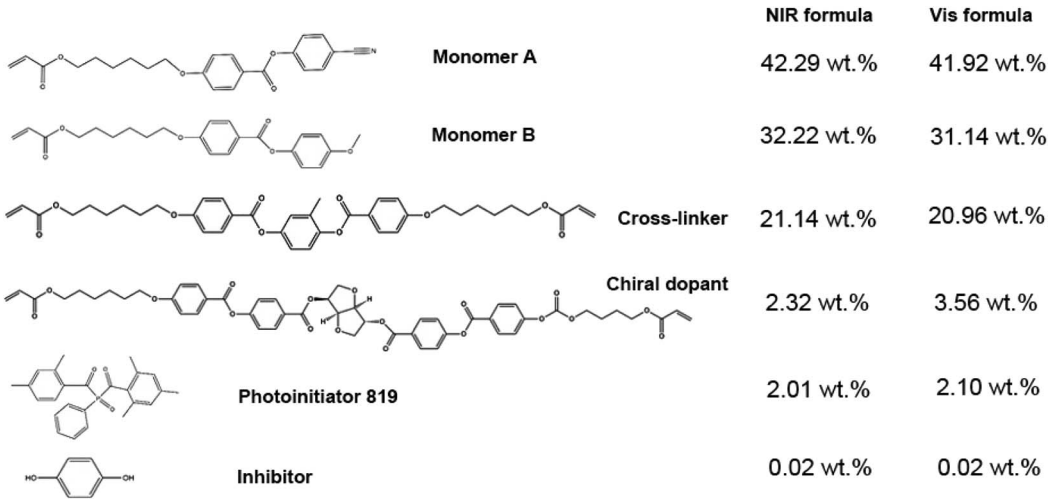

Fig. 2 Formulae of CLCP with near infrared (NIR) and visible (Vis) reflection bands.

to 1120 nm, but was about 35% in the visible range from 390 to 750 nm.

On the contrary, one of the near infrared (NIR) CLCP formulas reached about 37% in the same NIR range, but was below 10% in the same Vis range. The corresponding transmittance spectrum is shown in Fig. 3. Given that the infrared region is a large part of solar radiation energy, the NIR formula was selected as the functional unit of the adjustable smart window for indoor temperature control.

Different from other similar CLC formulas, an adequate addition of the inhibitor, namely hydroquinone, was also introduced to restrict free radicals within the local region. In general, light irradiation can induce a rapid decomposition of photo initiators to produce plenty of free radicals. These free radicals will couple with monomer units into active centers to promote the propagation of polymerization or a cross-linking reaction. As shown in Fig. 1, the introduced inhibitors will effectively control the amount and activity of the photo-initiated active centers in the limited lighting region against the diffusion and initiation of those generated free radicals. Finally, the optimum concentration of hydroquinone in the two CLC formulas, 0.02 wt%, was fixed after pre-experiments. It is very helpful to complete a local *in situ* polymerization for the limited polymerized and cross-linked CLCP. Of course, a normal CLC formula without an inhibitor was also tested. It was found that polymerization still occurred inside the dark region to form a whole cured film, rather than separate microsheets.

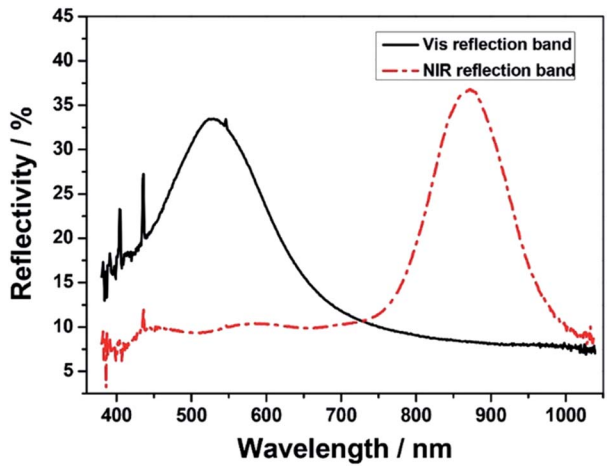

Fig. 3 UV-Vis-NIR reflection spectra of two fully cured CLCP films with Vis and NIR reflection bands.

Optimization of preparation conditions

The ability to control the presupposed polymerizing region corresponding to every hole of the pattern photomask becomes very critical. Expect for the inhibitor, the other key preparation parameters, including injecting temperature, photoirradiation intensity, irradiation time, irradiation distance, and "curing" temperature, were determined for the employed LPISP.

In the two CLC formulas, the cross-linker, monomer A and monomer B were tested to obtain their clear point temperatures, namely 70 °C, 78 °C and 62 °C, respectively. So 80 °C was set as the preheating temperature or injecting temperature in order to make all the components stable in the isotropic flowing state.

In fact, having only the inhibitor is not enough to thoroughly limit the diffusion and initiation of free radicals. According to the mechanism for the photo-initiated free radical polymerization, the photoirradiation intensity determines the rate of photoinitiator decomposition, and the irradiation time does influence the amount of free radicals generated from the initiator. By contrast experiments, with a fixed irradiation distance of 5 cm, the 0.1 W cm^{-2} and 30 seconds of photoirradiation were finally chosen as the optimum conditions. Both the higher intensity (*e.g.*, 0.5 W cm^{-2}) and longer time (*e.g.*, 50 seconds) will make the CLC solution fully polymerized to form a continuous polymeric film. Moreover, to form the CLCP microsheets, it also must make sure that the LC mixture is stable in the cholesteric state. This means that those hot CLC mixtures (~80

°C) need to be cooled down below the clearing temperature prior to photoirradiation after injection into the LC cell. As a testing result, two CLC formulas had close clear point temperatures, namely 55 °C (NIR formula) and 56 °C (Vis formula). We also performed optical measurements of the photo-initiated CLC prepolymers in the LC cell at different phase-stabilized temperatures or assisted "curing" temperatures. Fig. 4 showed that all the assisted "curing" temperatures below the close clearing temperature of 55 °C can contribute to the expected reflection band. A higher and narrower reflection band will appear as the temperature approached closer to the clearing temperature. Nevertheless, at 60 °C or 70 °C, the LC mixture will degenerate to become isotropic without a NIR reflective helical structure.

Morphologic control of CLCP microsheets

First, the use of an LC cell can be viewed as a morphologic control condition of the CLCP microsheet forming. In particular, the low depth width ratio between the cell gap and the irradiation region determined by the light hole will lead to the production of flat CLCP microsheets.

Second, the photomask is really a determined factor to the size and shape of the CLCP microsheets. In the initial experiments, the photomask with the regular circle holes (hole size: 10 μm) was used, but its photo-curing effect was not expected. Subsequently, larger hole sizes, namely 15, 30 and 60 μm, were tested in turn.

Fig. 5 presents almost circular microparticles with diameters of 45.7, 44.4, and 90.0 μm, respectively. All these final particles were larger than their corresponding light holes, particularly 15 μm of the hole size. It may contribute to the diffusion of free radicals or active centers in the LC mixture solution. In addition, the thickness of the cover glass plate (1.1 mm) between the photomask and the liquid crystal content is also significant. Here, the light refraction or diffraction may cause a larger microsheet boundary.

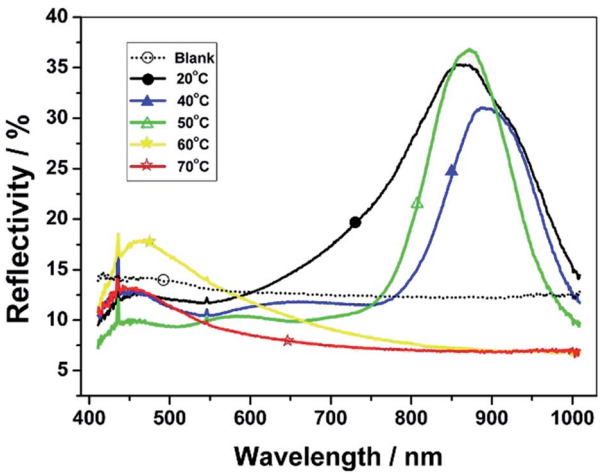

Fig. 4 UV-Vis-NIR reflection spectra of CLC prepolymers with NIR reflection bands under fixed photoirradiation conditions (0.1 W cm^2; 30 seconds) at different phase-stabilized temperatures.

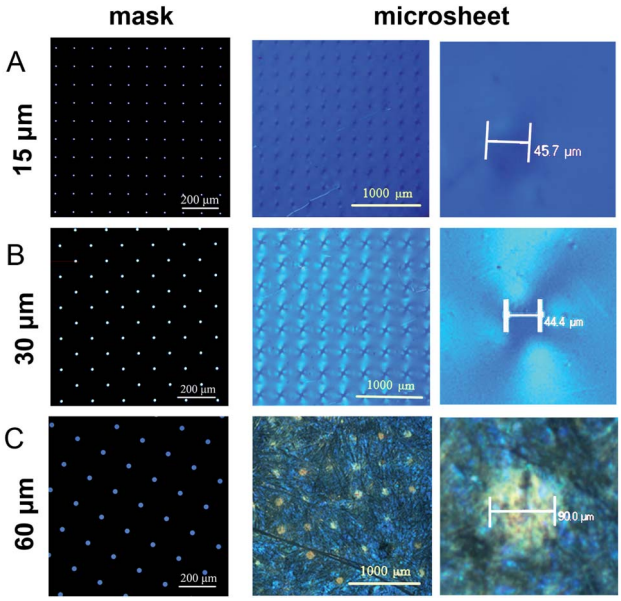

Fig. 5 POM images of photomasks (the first column) and corresponding CLCP microsheets (the second and third columns): (A) photomask with regular circle holes (size: 15 μm; pitch: 250 μm); (B) photomask with regular circle holes (size: 30 μm; pitch: 300 μm); (C) photomask with regular circle holes (size: 60 μm; pitch: 350 μm).

Fig. 6 provides more detailed morphology photographs on the resulting circular microparticles. Obviously, these microsheets were uniform and independent, not cross-linked to each other. With the polarized light, these locally formed microsheets appeared in obvious refraction, totally different from the ambient dichloromethane media (see Fig. 6C). It indicated that the *in situ* polymerization could maintain its original cholesteric phase with the presupposed reflection band. In Fig. 6E, a perfectly circular particle appeared in the center and behaved with the melon-like embossment. At the macroscopic level, these microsheets were certainly produced in line with our predictions. Both their shapes and sizes fully satisfied the morphology needed for further applications.

Furthermore, we tried to apply few special photomasks with different hole shapes and same hole areas for controlling the microsheet shape. As shown in Fig. 7, the formed microsheets had a regular shape similar to the corresponding light holes. Both the triangular and oval-shaped microsheets with sharp outlines were obviously obtained and arrayed in an orderly manner. By comparison, the pentagon microsheets had curved edges much more approximate to that of the circle. It is well-known that free radicals or active centers can diffuse circlewise and randomly from the microscale irradiation region into the adjacent LC solution. In addition, the diffraction between the photomask and liquid crystal may also expand the actual irradiation region. Both the above two factors will smoothen their edges, particularly for the larger microsheets.

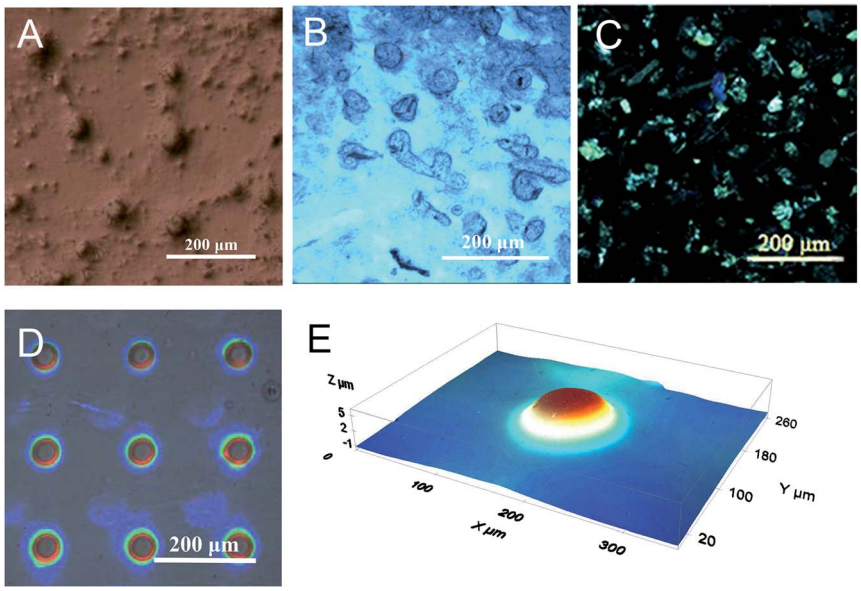

Fig. 6 Optical images of the CLCP microsheets molded by a photomask with regular circle holes (size: 60 μm; pitch: 350 μm): optical micrograph (A) and POM profiles (B and C) of the filtered microsheets in dichloromethane; 3D surface profiles of the locally formed microsheets (D and E).

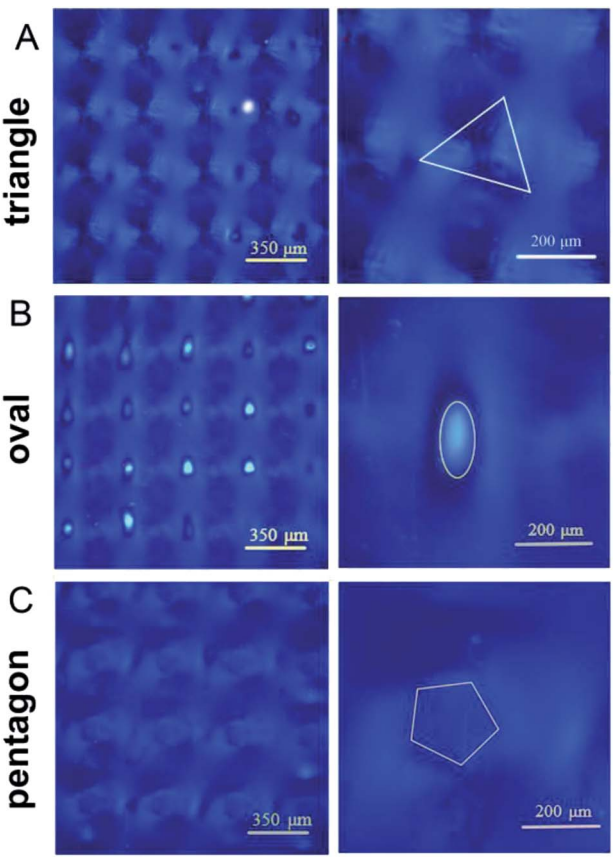

Fig. 7 POM images of the CLCP microsheets molded by photomasks with different hole shapes: (A) regular triangle hole (side length: 81 μm); (B) oval hole (long axis: 85 μm; short axis: 42 μm); (C) circle-inscribed pentagon hole (diameter: 102 μm).

Conclusions

In summary, a one-step formation technology to produce uniform CLCP microsheets was developed for a high-quality LC smart window. Hereinto, the optimization of the LC formula, photomask, and preparation conditions can surely contribute to a rapid and controllable LPISP of the CLC mixture within the local irradiation region to adjust the size and shape of the resulting microsheets. In addition to different sizes, triangular, elliptical, and pentagon microsheets were also successfully obtained. It is cheap, continuous, recyclable and a promising technology to motivate the industrial mass fabrication of the CLCP microsheet-suspended smart window.

Conflicts of interest

There are no conflicts to declare.

Acknowledgements

This work was financially supported by the National Natural Science Foundation of China (No. 51773069, 51703070 and 51673007), NSFC-Guangdong joint fund (No. U1501244), NSFC-NWO cooperation project (No. 51561135014), Guangdong Innovative Research Team Program (No. 2013C102), Guangdong Provincial Key Laboratory of Optical Information Materials and Technology (No. 2017B030301007), Startup funding from South China Normal University (No. 8S0134), MOE International Laboratory for Optical Information Technologies and the 111 Project.

Notes and references

1 F. Asdrubali and G. Baldinelli, *Build. Simul.*, 2009, **2**, 75.
2 B. A. Korgel, *Nature*, 2013, **500**, 278.
3 H. Khandelwal, A. P. H. J. Schenning and M. G. Debije, *Adv. Energy Mater.*, 2017, **7**, 1602209.
4 E. Hammarberg and A. Roos, *Thin Solid Films*, 2003, **442**, 222.
5 T. Rosencrantz, H. Bülow-Hübe, B. Karlsson and A. Roos, *Sol. Energy Mater. Sol. Cells*, 2005, **89**, 249.
6 C. H. Cheng and J. M. Ting, *Thin Solid Films*, 2007, **516**, 203.
7 S. M. A. Durrani, E. E. Khawaja, A. M. Al-Shukri and M. F. Al-Kuhaili, *Energy Build.*, 2004, **36**, 891.
8 C. G. Granqvist, A. Azens, J. Isidorsson, M. Kharrazi, L. Kullman, T. Lindström, G. A. Niklasson, D. Rönnow, M. Mattsson Strømme, M. Veszelei and G. Vaivars, *Sol. Energy*, 1998, **63**, 199.
9 G. Cai, A. L. S. Eh, L. Ji and P. S. Lee, *Adv. Sustainable Syst.*, 2017, **1**, 1700074.
10 Z. Xu, W. Li, J. Huang, Q. Liu, X. Guo, W. Guo and X. Liu, *J. Mater. Chem. A*, 2018, **6**, 19584.
11 C. G. Granqvist, M. A. Arvizu, H. Y. Qu, R. T. Wen and G. A. Niklasson, *Surf. Coat. Technol.*, 2018, **357**, 619.
12 W. Feng, L. Zou, G. Gao, G. Wu, J. Shen and W. Li, *Sol. Energy Mater. Sol. Cells*, 2016, **144**, 316.
13 Y. Wang, E. L. Runnerstrom and D. J. Milliron, *Annu. Rev. Chem. Biomol. Eng.*, 2016, **7**, 283.
14 C. M. Lampert, *Mater. Today*, 2004, **7**, 28.
15 R. Baetens, B. P. Jelle and A. Gustavsen, *Sol. Energy Mater. Sol. Cells*, 2010, **94**, 87.
16 M. Kim, K. J. Park, S. Seok, J. M. Ok, H. T. Jung, J. Choe and D. H. Kim, *ACS Appl. Mater. Interfaces*, 2015, **7**, 17904.
17 H. Kakiuchida, M. Tazawa, K. Yoshimura and A. Ogiwara, *Sol. Energy Mater. Sol. Cells*, 2010, **94**, 1747.
18 R. Vergaz, J. M. Sanchez-Pena, D. Barrios, C. Vazquez and P. Contreras-Lallana, *Sol. Energy Mater. Sol. Cells*, 2008, **92**, 1483.
19 A. Ghosh, B. Norton and A. Duffy, *Appl. Energy*, 2015, **159**, 362.
20 I. Dierking, *Polym. Chem.*, 2010, **1**, 1153.
21 G. Tan, Y. H. Lee, F. Gou, H. Chen, Y. Huang, Y. F. Lan, C. Y. Tsai and S. T. Wu, *J. Phys. D: Appl. Phys.*, 2017, **50**, 493001.
22 J. Y. Park and H. K. Kim, *RSC Adv.*, 2018, **8**, 36549.
23 S. M. Guo, X. Liang, C. H. Zhang, M. Chen, C. Shen, L. Y. Zhang, X. Yuan, B. F. He and H. Yang, *ACS Appl. Mater. Interfaces*, 2017, **9**, 2942.
24 J. Murray, D. Ma and J. N. Munday, *ACS Photonics*, 2016, **4**, 1.
25 Z. Shi, L. Shao, F. Wang, F. Deng, Y. Liu and Y. Wang, *Liq. Cryst.*, 2018, **45**, 579.
26 X. Liang, M. Chen, G. Chen, C. Li, C. Han, J. Zhang, J. Zhang, L. Zhang and H. Yang, *Polymer*, 2018, **146**, 161.
27 M. Kim, K. J. Park, S. Seok, J. M. Ok, H. T. Jung, J. Choe and D. H. Kim, *ACS Appl. Mater. Interfaces*, 2015, **7**, 17904.
28 D. Liu, C. W. Bastiaansen, J. M. den Toonder and D. J. Broer, *Angew. Chem., Int. Ed.*, 2012, **51**, 892.
29 D. Liu, C. W. Bastiaansen, J. M. den Toonder and D. J. Broer, *Macromolecules*, 2012, **45**, 8005.
30 J. Xiang, Y. Li, Q. Li, D. A. Paterson, J. M. Storey, C. T. Imrie and O. D. Lavrentovich, *Adv. Mater.*, 2015, **27**, 3014.
31 L. T. de Haan, V. Gimenez-Pinto, A. Konya, T. S. Nguyen, J. M. Verjans, C. Sánchez-Somolinos, J. V. Selinger, R. L. Selinger, D. J. Broer and A. P. Schenning, *Adv. Funct. Mater.*, 2014, **24**, 1251.
32 J. L. Fergason, *Mol. Cryst. Liq. Cryst.*, 1966, **1**, 293.
33 C. W. Oseen, *Trans. Faraday Soc.*, 1933, **29**, 883.